


1-6-2021

Probing the Effects of Heterogeneous Oxidative Modifications on the Stability of Cytochrome

Victor Yin

Lars Konermann

Follow this and additional works at: <https://ir.lib.uwo.ca/chempub>

 Part of the [Chemistry Commons](#)

Citation of this paper:

Yin, Victor and Konermann, Lars, "Probing the Effects of Heterogeneous Oxidative Modifications on the Stability of Cytochrome" (2021). *Chemistry Publications*. 234.
<https://ir.lib.uwo.ca/chempub/234>

Invited Contribution for Sarah Trimpin (2019 Biemann Medal) JASMS Special Issue

**Probing the Effects of Heterogeneous Oxidative
Modifications on the Stability of Cytochrome *c* in Solution
and in the Gas Phase**

Victor Yin and Lars Konermann*

*Department of Chemistry, The University of Western Ontario, London, Ontario,
N6A 5B7, Canada*

* corresponding author: konerman@uwo.ca

Funding was provided by the Natural Sciences and Engineering Research Council of Canada (RGPIN-2018-04243).

ABSTRACT: Covalent modifications by reactive oxygen species can modulate the function and stability of proteins. Thermal unfolding experiments in solution are a standard tool for probing oxidation-induced stability changes. Complementary to such solution investigations, the stability of electrosprayed protein ions can be assessed in the gas phase by collision-induced unfolding (CIU) and ion mobility spectrometry. A question that remains to be explored is whether oxidation-induced stability alterations in solution are mirrored by the CIU behavior of gaseous protein ions. Here we address this question using chloramine-T-oxidized cytochrome *c* (CT-cyt *c*) as a model system. CT-cyt *c* comprises various proteoforms that have undergone MetO formation (+16 Da) and Lys carbonylation (LysCH₂-NH₂ → LysCHO, -1 Da). We found that CT-cyt *c* in solution was destabilized, with a ~5 °C reduced melting temperature compared to unmodified controls. Surprisingly, CIU experiments revealed the opposite trend, i.e., a stabilization of CT-cyt *c* in the gas phase. To pinpoint the source of this effect, we performed proteoform-resolved CIU on CT-cyt *c* fractions that had been separated by cation exchange chromatography. In this way it was possible to identify MetO formation at residue 80 as the key modification responsible for stabilization in the gas phase. Possibly, this effect is caused by newly formed contacts of the sulfoxide with aromatic residues in the protein core. Overall, our results demonstrate that oxidative modifications can affect protein stability in solution and in the gas phase very differently.

Atomically resolved structural data for proteins in solution or in the solid state can be obtained by X-ray crystallography, NMR spectroscopy and cryo-electron microscopy. Mass spectrometry (MS) and ion mobility spectrometry (IMS) offer complementary avenues. Prerequisite for the application of these vacuum techniques is the capability to generate intact gaseous protein ions [1]. Electrospray ionization (ESI) [2] and matrix-assisted laser desorption/ionization (MALDI) [3] represent key techniques for this purpose, but new ionization methods continue to emerge [4-8]. Particularly interesting is recent work by Trimpin et al. [8] which demonstrated that gaseous protein ions can be generated without the aid of lasers, heat, or voltages.

The amino acids in natively folded proteins are closely packed and engaged in H-bonds, salt bridges, van der Waals interactions, and hydrophobic contacts [9]. Covalent modifications can upset this interaction network, destabilize the native state, and render proteins non-functional [10]. One avenue to introduce such modifications involves reactive oxygen species, such as O_2^- , HO_2^\bullet , H_2O_2 , and HO^\bullet [11-14]. Methionine conversion to sulfoxide (MetO) is particularly common [15-18], but oxidation can also affect many other residues [19,20]. The accumulation of oxidized proteins plays a key role for aging-related pathologies [21] such as Alzheimer's and other neurodegenerative diseases [22,23]. In addition, oxidation compromises the efficacy of protein therapeutics [16,18,24]. Understanding oxidation-related effects on protein structure and stability, therefore, is an important goal with far-reaching repercussions.

Oxidation-induced stability changes in solution can be studied using thermal [15,18,25,26] or chemical [27,28] unfolding experiments. These studies involve protein exposure to heat or chemical denaturants. Optical tools can then be used to probe unfolding profiles, e.g., circular dichroism (CD) spectroscopy at 222 nm which reports on α -helicity [29]. The melting temperature T_M marks the unfolding midpoint and is a measure of protein stability [9,30,31]. Oxidative modifications usually destabilize proteins in solution, inducing shifts to lower T_M [15,18,25-28].

In addition to the aforementioned solution studies, there is considerable interest in examining proteins in a solvent-free environment. “Native” ESI can generate gaseous biomolecular ions that retain solution-like structures and interactions [7,32-36]. Somewhat analogous to thermal unfolding in solution [15,18,25,26,30], these gaseous protein ions can be subjected to collisional heating, causing them to undergo collision-induced unfolding (CIU). The structural changes triggered in this way are detectable by IMS [37,38].

It is an interesting question whether gas phase stabilities correlate with the protein behavior in solution [39,40]. A number of studies indicate that this indeed appears to be the case. For example, enzyme-inhibitor binding stabilities in solution were consistent with trends seen in collision-induced dissociation (CID) studies [41], ligand-induced stabilization effects were mirrored in the gas phase [42], and CIU energetics were shown to be correlated with solution structures [38]. Correlation between solution and gas phase behavior was also demonstrated in surface-induced dissociation (SID) experiments on multi-protein assemblies [36], and blackbody infrared dissociation (BIRD) studies on protein-lipid complexes [43]. On the other hand, the absence of solvent can have profound effects on inter- and intramolecular contacts [44]. Hydrophobic interactions are weakened [45], while electrostatic contacts are strengthened in the absence of water [46]. These factors can lead to disparities between solution and gas phase stabilities [46]. Overall, much remains to be learned about the relationship between protein stability *in vitro* and *in vacuo*. Particular knowledge gaps persist when it comes to the question how oxidative modifications affect the stability of gaseous proteins.

Oxidative modifications of the heme protein cytochrome *c* (cyt *c*) have attracted a lot of attention in recent years [47-56]. The canonical function of cyt *c* is to shuttle electrons in the respiratory chain [57]. In addition, cyt *c* acts as a peroxidase, i.e., an enzyme that catalyzes the oxidation of organic substrates by H₂O₂ [58]. Cyt *c*-catalyzed oxidation of cardiolipin in

mitochondria plays a key role during apoptosis [59-62]. The peroxidase activity of native cyt *c* is low. It is only after specific oxidation events that the protein becomes fully active [47-54,63,64]. This gain of function contrasts the aforementioned scenarios where oxidation events interfere with protein activity.

The most common method for producing peroxidase-active cyt *c in vitro* is by exposure to chloramine-T (CT) [47,51,53,54], a mild oxidant that releases OCl⁻ [65]. We recently conducted a detailed MS characterization of CT-treated cyt *c* (CT-cyt *c*) [63]. The protein was found to be highly heterogeneous, with MetO formation at zero, one, or two methionines (Met80 and Met65). In addition, CT-cyt *c* showed Lys carbonylation in the range of Lys72/73 and Lys53/55 (Figure 1) [63]. Lys carbonylation to amino adipic semialdehyde is associated with $\Delta M = -1$ Da (LysCH₂-NH₂ → LysCHO) [66,67]. This type of modification is easily missed because of its small mass shift, loss of a charged site, and abrogation of tryptic cleavage. In particular, the presence of LysCHO in CT-cyt *c* had been overlooked until recently [63]. Both MetO and LysCHO are well-known markers for oxidative damage in environmentally stressed proteins and protein therapeutics [67,68]. Therefore, CT-cyt *c* represents as a convenient model system for probing the effects of these modifications on protein structure and stability.

Here we characterize the effects of oxidative modifications in CT-cyt *c* on the stability of the protein in solution and in the gas phase. We find that although the solution stability of the protein is reduced after oxidation, gas phase data show an increase in stability. We conclude that the solution properties of oxidatively modified proteins are not necessarily reflected in their CIU behavior.

Materials and Methods

Materials. Cyt *c* (equine heart), CT (N-chloro-4-toluosulfonamide), and Tris base (2-amino-2-(hydroxymethyl)-1,3-propanediol) were supplied by MilliporeSigma (St. Louis, MO). All other chemicals were supplied by Fisher Scientific (Nepean, ON) or Caledon Laboratories (Georgetown, ON). Centrifuge filters (Amicon Ultra 0.5, 10 kDa MWCO) were supplied by Millipore Sigma, and used according to manufacturer instructions (15 min at 13,000 g).

Protein Oxidation. CT-cyt *c* was prepared as described [63], with minor modifications. 500 μM cyt *c* was incubated with 2.5 mM CT in 50 mM Tris (pH 8.4) for 60 min at 22 °C. Oxidation was quenched by five serial exchanges into 10 mM ammonium acetate using Amicon filters. The resulting proteoform mixture was fractionated using a 5 mL SCX HiTrap SP cartridge (GE Healthcare). Samples were eluted using a zero to 500 mM ammonium acetate gradient (pH 9).

Thermal Unfolding. Solution phase unfolding was monitored by CD spectroscopy at 222 nm using a J-810 spectropolarimeter (JASCO, Easton, MD). Samples were prepared as 10 μM protein in 50 mM potassium phosphate buffer (pH 7.4). Heating was performed from 20 to 100 °C at a rate of 1 °C min^{-1} . The melting temperature (T_M) and enthalpy of unfolding (ΔH) were extracted by fitting the CD_{222} profiles using [30]

$$CD_{222} = \frac{(y_N + m_N T) + (y_U + m_U T) \exp(-\Delta G/RT)}{1 + \exp(-\Delta G/RT)} \quad (1)$$

where T is the temperature in Kelvin and $\Delta G = \Delta H(1 - T/T_M)$, while $(y_N + m_N T)$ and $(y_U + m_U T)$ represent the pre- and post-transition baselines, respectively. The fraction of unfolded protein in solution (F_{u_sol}) was calculated as [69]

$$F_{u_sol} = \frac{\exp(-\Delta G/RT)}{1+\exp(-\Delta G/RT)} \quad (2)$$

There was no evidence of aggregation, as seen from the absence of precipitated protein in the heated samples.

Mass Spectrometry. MS experiments were performed on a Waters SYNAPT G2-Si instrument in positive ion mode (Waters, Milford, MA). Samples were prepared as 10 μ M protein in either 10 mM ammonium acetate for native ESI, or 50/50/0.1 H₂O/methanol/formic acid for denaturing conditions, and infused at 5 μ L min⁻¹. Travelling wave IMS experiments were performed in sensitivity mode with N₂ as buffer gas. Instrument parameters were tuned to maintain minimal ion activation prior to deliberate activation for CIU (Table S1). CIU was performed by varying the trap collision energy, with Ar as collision gas. IMS profiles of 8+ ions were extracted using TWIMextract [70]. IMS drift times were converted into effective helium collision cross sections (Ω) [71]. CIU curves were expressed as fraction unfolded in vacuum (F_{u_vac}), defined as

$$F_{u_vac} = \frac{\langle\Omega\rangle - \langle\Omega_N\rangle}{\langle\Omega_U\rangle - \langle\Omega_N\rangle} \quad (3)$$

where $\langle\Omega\rangle$ is the average Ω at a given trap collision energy. $\langle\Omega_N\rangle$ and $\langle\Omega_U\rangle$ are the average Ω values measured for minimum (1 V) and maximum collisional excitation (20 V), respectively. All CIU experiments were performed in triplicate, with independent Ω calibrations for each replicate. Error bars represent standard deviations. Simulated isotope distributions of Fe(III) cyt *c* were generated using the UCSF ProteinProspector web server.

Results and Discussion

Chromatographic Separation of Proteoforms. Exposure of *cyt c* to CT produces a mix of oxidation products that are modified at Met and Lys side chains [63]. The complexity of these CT-*cyt c* samples can be alleviated by using strong cation exchange (SCX) chromatography. Under the conditions used here, three major SCX fractions were obtained (I, II, and III in Figure 2A). The SCX retention time of fraction I was virtually identical to that of unmodified control samples which had not been exposed to CT.

A cursory glance at the mass distributions of the three CT-*cyt c* fractions suggests that they are quite similar to one another. Each fraction showed three dominant signals, corresponding to 0, 1, and 2 MetO modifications (approximately +0, +16, +32 Da, Figure 2B-D). The 1 MetO species were previously shown to be oxidized at Met80, while the 2 MetO proteoforms are modified at Met80 and Met65 [63]. However, close examination and comparison with modeled isotope distributions reveals additional mass shifts of -2, -1, and -0 Da for fractions III, II, and I. These negative shifts are attributable to the presence of 2, 1, and 0 LysCHO sites. Proteoforms with a -1 Da shift are carbonylated at Lys72/73, while -2 Da species are additionally modified at Lys53/55 [63]. The progressive loss of positive charge for these proteoforms is consistent with their SCX retention behavior, keeping in mind that SCX separates proteins based on their cationic character in solution. Specifically, fraction III which has lost the most charge due to two $\text{Lys}^+ \rightarrow \text{LysCHO}$ conversion events was most weakly retained (Figure 2A).

The observation that all three fractions share virtually the same MetO oxidation pattern (Figure 2B-D) indicates that Met oxidation and Lys carbonylation occur independently of one another during *cyt c* exposure to CT. The inability of SCX to separate proteoforms with different MetO content reflects the fact that this type of modification does not affect the protein charge.

In summary, the CT-cyt *c* preparations examined here represent a mix of proteoforms that contain 0, 1, or 2 MetO sites, as well as 0, 1, or 2 LysCHO modifications. SCX allows separation into three fractions that are pure with respect to LysCHO content, but heterogeneous in the number of MetO sites. The separation of CT-cyt *c* into three fractions facilitates the subsequent experiments, compared to investigations on unseparated samples.

Stability of CT-cyt *c* in Solution. Unfolding experiments were performed to establish how CT-induced oxidative modifications affect the stability of cyt *c* in solution (Figure 3). Instead of using chemical denaturation [27,28] we chose thermal unfolding assays [15,18,25,26] to allow a direct comparison with gas phase CIU experiments (discussed below), keeping in mind that both techniques probe the protein response to heat. The thermodynamic parameters measured for unmodified cyt *c* were $T_M = 86.8 \pm 0.2$ °C and $\Delta H = 493 \pm 20$ kJ mol⁻¹. The former agrees with literature data within 1 °C [72]. Previous work reported a somewhat lower ΔH (400 kJ mol⁻¹ [73]) but that earlier study used acidic solutions, while our experiments were performed at pH 7.4. Compared to the unmodified controls, all three CT-cyt *c* fractions showed a substantial decrease in both T_M (ca. 5 °C) and ΔH (ca. 50%), revealing that CT-induced oxidative modifications reduce the stability of the protein in solution (Table 1). The stability reduction seen here for CT-cyt *c* is reminiscent of data reported previously for other oxidatively modified proteins [15,18,25-28].

Interestingly, stability differences between the individual oxidized fractions I, II, and III were small, evident from their almost superimposable unfolding profiles (Figure 3). As discussed above, the three fractions only differ in the number of modified Lys residues (0, 1, 2 LysCHO for fractions I, II, III), while they share very similar MetO compositions. From this, one can conclude that LysCHO formation does not significantly affect the protein stability in solution, consistent with the location of these modifications on side chains that protrude into the solvent (Figure 1A).

Instead, the major stability difference between unmodified *cyt c* and CT-*cyt c* are attributable to MetO formation. Oxidation of the deeply buried Met80 is expected to be particularly disruptive because it ruptures the distal Fe-sulfur bond and interferes with side chain packing in the protein core [74]. Met65 modifications likely affect the protein stability to a lesser extent, because this residue is located close to the protein surface without any critical side chain contacts (Figure 1A).

ESI Charge States of CT-*cyt c*. Because the formation of each LysCHO is concomitant with the loss of a basic (protonatable) site, one might expect that the ESI charge state distribution of $[M + zH]^{z+}$ ions could be affected by LysCHO formation. However, native ESI mass spectra of unmodified controls and fractions I-III were very similar to one another, with charge state distributions dominated by 8+/7+ ions. In contrast, spectra acquired under denaturing conditions exhibited slight shifts to lower charge states, from maxima of 17+/16+ for unmodified *cyt c* and fraction I, down to 16+/15+ for fraction III (Figure 4).

Native ESI proceeds according to the charged residue model (CRM), where protein ions are released upon droplet evaporation to dryness. Charge states generated under these conditions are close to those of protein-sized water droplets at the Rayleigh limit ($z_R \approx 7.9$ for *cyt c*) [75-77]. Thus, CRM charge states of globular proteins are governed by their surface area, rather than the number of basic sites [78]. The fact that native ESI generates very similar charge state distributions for unmodified and CT-*cyt c* indicates that the covalent modifications encountered here do not dramatically alter the overall compactness of the protein. This view is consistent with native ESI Ω values which are very similar for all proteoforms (see below and Table S2).

The situation is different under denaturing ESI conditions, where protein ions likely form according to the chain ejection mechanism (CEM) [77]. The CEM proceeds with gradual ejection of extended protein chains from the droplet surface, in concert with the equilibration of mobile H^+

between the droplet and its protein appendage. Any factor that decreases the effective basicity of the protein will compromise the capability of the chain to compete for H^+ during ejection. The slight shift to lower charge states seen for fraction III under denaturing ESI conditions therefore likely reflects the loss of basic sites due to conversion of two Lys to LysCHO (Figure 4). In summary, the ESI charge state distributions of the various proteoforms are consistent with current views of the ESI process under native and denaturing conditions [75-77].

Native ESI Gas Phase Conformations of CT-cyt *c*. We initially probed the conformations of unmodified 8+ cyt *c* ions and fractions I-III with minimum collisional excitation (collision energy 1 V) in an effort to preserve solution-like structures in the gas phase [7,32-36]. Figure 5A-D displays the resulting IMS data in a MetO-averaged fashion. The unmodified control protein displayed a single dominant feature centered at $\sim 1350 \text{ \AA}^2$, consistent with previous reports [79-82]. Virtually the same IMS behavior was seen for fractions I-III (Figure 5A-D, Table S2). These native ESI data reaffirm that CT-induced oxidation does *not* induce large-scale global alterations of the protein structure, although minor perturbations are known to take place [54,63]. Our IMS data are quite different from those of a recent report [55] where it was concluded that oxidative modifications cause a significant compaction of cyt *c*. The IMS data of ref. [55] showed multiple peaks for both unmodified and oxidized cyt *c*, suggesting that the ions had undergone partial CIU. In contrast, our native ESI-IMS data (and previous studies [79-82]) are dominated by single IMS features, presumably corresponding to solution-like conformations that were not significantly affected by collisional heating. Unfortunately, the IMS data of ref. [55] were not Ω -calibrated, rendering a direct comparison with our results difficult.

Gas Phase Stability of CT-cyt *c*. While the aforementioned IMS experiments avoided collisional excitation, we will now discuss the CIU behavior of the various CT-cyt *c* proteoforms to assess their gas phase stabilities. Similar to unfolding in solution, the extent of structural perturbation in these CIU experiments can be expressed as a fraction unfolded (F_{u_vac} , Equation 3). IMS/MS is capable of tracking the IMS profiles of each individual MetO and LysCHO species (see below). In contrast, the solution unfolding experiments of Figure 3 could only probe the behavior of fractions I-III in a MetO-averaged fashion. To allow a direct comparison with those solution data, we initially compiled MetO-averaged CIU data (Figure 5).

Raising the collision energy from 1 V to 20 V resulted in significant gas phase unfolding for all 8+ species, transforming the “native” ($\sim 1350 \text{ \AA}^2$) IMS distributions into unimodal profiles centered at $\sim 1730 \text{ \AA}^2$ (Figure 5, Table S2). Although the $\langle \Omega \rangle$ values of CT-cyt *c* at the lowest and highest collision energies were very similar to the unmodified protein, there were clear differences in the intermediate energy regime. At 7 V all of the IMS profiles had maxima around 1400 \AA^2 . In addition, the unmodified control exhibited a major feature at $\sim 1700 \text{ \AA}^2$, which is close to the fully unfolded protein (marked by the red arrow in Figure 5E). This unfolded feature was also seen for fractions I-III, but at much lower intensities (Figure 5F-H). Upon raising the collision energy to 9V the IMS distribution of the unmodified control was completely dominated by this $\sim 1700 \text{ \AA}^2$ feature (Figure 5I), while more compact conformers (around 1500 \AA^2) persisted for fractions I-III (see arrows in Figure 5J-L). No major differences are seen when comparing the CIU data for fractions I-III among each other.

Overall, our data reveal that the unmodified control protein is more susceptible to CIU than fractions I-III. This effect is also apparent from the F_{u_vac} profiles (Figure 5Q) which have a midpoint at 0.5 V – 1 V lower collision energies for unmodified cyt *c* than for fraction I-III. Based on these F_{u_vac} profiles alone it might be difficult to discern the differences between unmodified

cyt *c* and fractions I-III; however, the dissimilarities seen in the IMS distribution for intermediate collision energies are striking (Figure 5E-L). The observed oxidation-induced *stabilization* of cyt *c* in the gas phase (Figure 5) contrasts the *destabilization* observed in solution (Figure 3).

Proteoform-Resolved CIU Analysis. More detailed insights into the role of each modification can be obtained by extracting IMS profiles of individual proteoforms. The three MetO variants are separable by their mass differences (+0, +16, +32 Da), while the LysCHO variants (0, -1, -2 Da) can be resolved using SCX fractionation. To facilitate the following discussion, we will identify proteoforms as $KmMn$, where m and n are the number of LysCHO and MetO, respectively. For example, K0M0 represents unmodified cyt *c*, while K2M1 refers to the proteoform containing 2 LysCHO and 1 MetO.

To investigate the effects of MetO in the absence of LysCHO modifications we probed the K0M n series ($n = 0, 1, 2$, Figure 6). At intermediate collision energies, both K0M1 and K0M2 had structures that were significantly more compact than for K0M0, evident from the features highlighted with arrows in Figure 6D-I. Also, the midpoints of the K0M1 and K0M2 CIU profiles are ~ 1 V higher than that of K0M0, while the former two are virtually superimposable (Figure 6M). From these data it can be concluded that oxidation of Met80 (in K0M1) enhances the gas phase stability of the protein, while the additional oxidation of Met65 (in K0M2) has no discernible effect.

A similar analysis was conducted to investigate the effects of LysCHO modifications by focusing on the $KmM1$ series ($m = 0, 1, 2$, Figure 7). The IMS distributions (Figure 7A-L) and CIU profiles (Figure 7M) for these three species were very similar across all collision energies, suggesting that LysCHO formation only has minor effects on the gas phase stability of cyt *c*. The last aspect is consistent with the behavior in solution (Figure 3), where the number of LysCHO

also has a negligible effect on stability. This is in stark contrast to MetO formation at residue 80 which greatly affects the properties of cyt *c*, giving rise to opposing stability trends in solution and in the gas phase.

Conclusions

Our results reveal that CT-induced oxidation affects the cyt *c* stability in solution and in the gas phase quite differently. In solution, CT-cyt *c* has a melting point that is ~ 5 °C lower than that of unmodified cyt *c*, implying large-scale destabilization. In the gas phase, oxidative modifications cause a small but distinct stabilization, evident from a ~ 1 V shift to higher CIU voltages. Our results indicate that both of these effects can be attributed largely to MetO formation of Met80, a residue that is deeply buried and represents the distal heme ligand in the native state [74]. The effects of other CT-induced oxidative modifications on protein stability are less pronounced (MetO formation at Met65, and LysCHO formation at Lys72/73 and Lys53/55). The lack of major changes following modification of these other sites is consistent with their solvent-exposed locations which allow covalent modifications to be accommodated without disrupting the side chain packing in the core (Figure 1A).

The observation that Met80 oxidation reduces the protein stability in *solution* is consistent with a wide range of observations on other oxidatively modified proteins, reflecting the fact that oxidation events usually perturb steric interactions, polarity, hydrophobicity, etc. [15,18,25-28]. In cyt *c* the conversion of Met80 to MetO additionally ruptures the distal Met-Fe bond [47,51,53,54]. It seems surprising, therefore, that this modification would render the protein more resilient to CIU in the gas phase. One possible explanation is the formation of new bonds after conversion of Met80 to MetO. Recent work has shown that the partially positive sulfur atom in MetO can

noncovalently bind to the partially negative π electron clouds of aromatic rings [83]. Several aromatic residues are relatively close to Met80 (Trp59, Tyr67, Phe82, Figure 1B), and thus it seems conceivable that the enhanced gas phase stability could be rooted in newly formed contacts of MetO with one of these sites. Interestingly, computer simulations predict that such MetO-aromatic contacts will be disfavored in water [84]. This could explain our observation of MetO-induced destabilization in solution vs. stabilization in the gas phase.

It is also somewhat surprising that Lys carbonylation does not have a destabilizing effect in the gas phase, keeping in mind the role of strengthened electrostatic contacts *in vacuo* and the likely involvement of Lys⁺ in salt bridges at the protein surface [46]. It is possible that the loss of basic sites due to LysCHO formation is compensated by other factors, such as dipole interactions of -CHO sites with positively charged moieties on the protein surface.

Overall, the results of this work highlight the fact that protein stability trends observed in solution are not always mirrored by the corresponding gaseous ions, consistent with the findings of several previous studies [44-46]. Investigating the origin of these different trends offers exciting opportunities to better understand the complex interplay of electrostatic and other noncovalent contacts in native and covalently modified proteins. It is hoped that future comparative solution/gas phase investigations will provide further insights into the molecular foundation of oxidation-induced alterations on protein function and stability.

Acknowledgments

The authors thank Lee-Ann Briere and E. Aisha Freeman for their technical assistance.

References

1. Covey, T.R., Thomson, B.A., Schneider, B.B.: Atmospheric Pressure Ion Sources. *Mass Spectrom. Rev.* **28**, 870-897 (2009)
2. Fenn, J.B.: Electrospray Wings for Molecular Elephants (Nobel Lecture). *Angew. Chem. Int. Ed.* **42**, 3871-3894 (2003)
3. Karas, M., Hillenkamp, F.: Laser Desorption Ionization of Proteins with Molecular Masses Exceeding 10 000 Daltons. *Anal. Chem.* **60**, 2299-2301 (1988)
4. Frey, B.L., Damon, D.E., Badu-Tawiah, A.K.: Emerging trends in paper spray mass spectrometry: Microsampling, storage, direct analysis, and applications. *Mass Spectrom. Rev.* **in press** (2020)
5. Brown, H.M., Pirro, V., Cooks, R.G.: From DESI to the MasSpec Pen: Ambient Ionization Mass Spectrometry for Tissue Analysis and Intraoperative Cancer Diagnosis. *Clin. Chem.* **64**, 628-630 (2018)
6. Susa, A.C., Lippens, J.L., Xia, Z., Loo, J.A., Campuzano, I.D.G., Williams, E.R.: Submicrometer Emitter ESI Tips for Native Mass Spectrometry of Membrane Proteins in Ionic and Nonionic Detergents. *J. Am. Soc. Mass Spectrom.* **29** (2018)
7. Chorev, D.S., Baker, L.A., Wu, D., Beilstein-Edmands, V., Rouse, S.L., Zeev-Ben-Mordehai, T., Jiko, C., Samsudin, F., Gerle, C., Khalid, S., Stewart, A.G., Matthews, S.J., Gruenewald, K., Robinson, C.V.: Protein assemblies ejected directly from native membranes yield complexes for mass spectrometry. *Science* **362**, 829-834 (2018)
8. Peacock, P.M., Zhang, W.J., Trimpin, S.: Advances in Ionization for Mass Spectrometry. *Anal. Chem.* **89**, 372-388 (2017)
9. Fersht, A.R. *Structure and Mechanism in Protein Science*; W. H. Freeman & Co.: New York, 1999.
10. Balchin, D., Hayer-Hartl, M., Hartl, F.U.: In vivo aspects of protein folding and quality control. *Science* **353**, 42 (2016)
11. Winkler, J.R., Gray, H.B.: Electron flow through biological molecules: does hole hopping protect proteins from oxidative damage? *Q. Rev. Biophys.* **48**, 411-420 (2015)
12. Nimse, S.B., Pal, D.: Free radicals, natural antioxidants, and their reaction mechanisms. *RSC Adv.* **5**, 27986-28006 (2015)
13. Kathiresan, M., English, A.M.: LC-MS/MS suggests that hole hopping in cytochrome c peroxidase protects its heme from oxidative modification by excess H₂O₂. *Chem. Sci.* **8**, 1152-1162 (2017)

14. Dalle-Donne, I., Rossi, R., Giustarini, D., Milzani, A., Colombo, R.: Protein carbonyl groups as biomarkers of oxidative stress. *Clin. Chim. Acta* **329**, 23-38 (2003)
15. Sigalov, A.B., Stern, L.J.: Oxidation of methionine residues affects the structure and stability of apolipoprotein A-I in reconstituted high density lipoprotein particles. *Chem. Phys. Lipids* **113**, 133-146 (2001)
16. Mo, J.J., Yan, Q.R., So, C.K., Soden, T., Lewis, M.J., Hu, P.: Understanding the Impact of Methionine Oxidation on the Biological Functions of IgG1 Antibodies Using Hydrogen/Deuterium Exchange Mass Spectrometry. *Anal. Chem.* **88**, 9495-9502 (2016)
17. Strickland, E.C., Geer, M.A., Tran, D.T., Adhikari, J., West, G.M., Dearmond, P.D., Xu, Y., Fitzgerald, M.C.: Thermodynamic analysis of protein-ligand binding interactions in complex biological mixtures using the stability of proteins from rates of oxidation. *Nat. Protocols* **8**, 148-61 (2012)
18. Buecheler, J.W., Winzer, M., Weber, C., Gieseler, H.: Oxidation-Induced Destabilization of Model Antibody-Drug Conjugates. *J. Pharm. Sci.* **108**, 1236-1245 (2019)
19. Xu, G., Chance, M.R.: Hydroxyl Radical-Mediated Modification of Proteins as Probes for Structural Proteomics. *Chem. Rev.* **107**, 3514-3543 (2007)
20. Saladino, J., Liu, M., Live, D., Sharp, J.S.: Aliphatic Peptidyl Hydroperoxides as a Source of Secondary Oxidation in Hydroxyl Radical Protein Footprinting. *J. Am. Soc. Mass Spectrom.* **20**, 1123-1126 (2009)
21. de Graff, A.M.R., Hazoglou, M.J., Dill, K.A.: Highly Charged Proteins: The Achilles' Heel of Aging Proteomes. *Structure* **24**, 329-336 (2016)
22. Pedersen, J.T., Chen, S.W., Borg, C.B., Ness, S., Bahl, J.M., Heegaard, N.H.H., Dobson, C.M., Hemmingsen, L., Cremades, N., Teilum, K.: Amyloid-beta and alpha-Synuclein Decrease the Level of Metal-Catalyzed Reactive Oxygen Species by Radical Scavenging and Redox Silencing. *J. Am. Chem. Soc.* **138**, 3966-3969 (2016)
23. Sultana, R., Boyd-Kimball, D., Poon, H.F., Cai, J., Pierce, W.M., Klein, J.B., Markesbery, W.R., Zhou, X.Z., Lu, K.P., Butterfield, D.A.: Oxidative modification and down-regulation of Pin1 in Alzheimer's disease hippocampus: A redox proteomics analysis. *Neurobiol. Aging* **27**, 918-925 (2006)
24. Bonnington, L., Lindner, I., Gilles, U., Kailich, T., Reusch, D., Bulau, P.: Application of Hydrogen/Deuterium Exchange-Mass Spectrometry to Biopharmaceutical Development Requirements: Improved Sensitivity to Detection of Conformational Changes. *Anal. Chem.* **89**, 8233-8237 (2017)
25. Mulinacci, F., Capelle, M.A.H., Gurny, R., Drake, A.F., Arvinte, T.: Stability of Human Growth Hormone: Influence of Methionine Oxidation on Thermal Folding. *J. Pharm. Sci.* **100**, 451-463 (2011)

26. Jayaraman, S., Gantz, D.L., Gursky, O.: Effects of protein oxidation on the structure and stability of model discoidal high-density lipoproteins. *Biochemistry* **47**, 3875-3882 (2008)
27. Walker, E.J., Bettinger, J.Q., Welle, K.A., Hryhorenko, J.R., Ghaemmaghami, S.: Global analysis of methionine oxidation provides a census of folding stabilities for the human proteome. *Proc. Natl. Acad. Sci. U. S. A.* **116**, 6081-6090 (2019)
28. Kim, Y.H., Berry, A.H., Spencer, D.S., Stites, W.E.: Comparing the effect on protein stability of methionine oxidation versus mutagenesis: steps toward engineering oxidative resistance in proteins. *Protein Eng.* **14**, 343-347 (2001)
29. Greenfield, N.J.: Methods to Estimate the Conformation of Proteins and Polypeptides from Circular Dichroism Data. *Anal. Biochem.* **235**, 1 - 10 (1996)
30. Swint, L., Robertson, A.D.: Thermodynamics of unfolding for turkey ovomucoid third domain: Thermal and chemical denaturation. *Protein Sci.* **2**, 2037-2049 (1993)
31. Geer, M.A., Fitzgerald, M.C.: Characterization of the *Saccharomyces cerevisiae* ATP-Interactome using the iTRAQ-SPROX Technique. *J. Am. Soc. Mass Spectrom.* **27**, 233-243 (2016)
32. Leney, A.C., Heck, A.J.R.: Native Mass Spectrometry: What is in the Name? *J. Am. Soc. Mass Spectrom.* **28**, 5-13 (2017)
33. Osterlund, N., Moons, R., Ilag, L.L., Sobott, F., Graslund, A.: Native Ion Mobility-Mass Spectrometry Reveals the Formation of beta-Barrel Shaped Amyloid-beta Hexamers in a Membrane-Mimicking Environment. *J. Am. Chem. Soc.* **141**, 10440-10450 (2019)
34. Kaddis, C.S., Loo, J.A.: Native Protein MS and Ion Mobility: Large Flying Proteins with ESI. *Anal. Chem.* **79**, 1779-1784 (2007)
35. Ashcroft, A.E.: Mass Spectrometry and the Amyloid Problem - How Far Can We Go in the Gas Phase? *J. Am. Soc. Mass Spectrom.* **21**, 1087-1096 (2010)
36. Harvey, S.R., Seffernick, J.T., Quintyn, R.S., Song, Y., Ju, Y., Yan, J., Sahasrabudhe, A.N., Norris, A., Zhou, M.W., Behrman, E.J., Lindert, S., Wysocki, V.H.: Relative interfacial cleavage energetics of protein complexes revealed by surface collisions. *Proc. Natl. Acad. Sci. U. S. A.* **116**, 8143-8148 (2019)
37. Clemmer, D.E., Jarrold, M.F.: Ion Mobility Measurements and their Applications to Clusters and Biomolecules. *J. Mass Spectrom.* **32**, 577-592 (1997)
38. Zhong, Y., Han, L., Ruotolo, B.T.: Collisional and Coulombic unfolding of gas-phase proteins: high correlation to their domain structures in solution. *Angew. Chem.* **53**, 9209-12 (2014)

39. Nouchikian, L., Lento, C., Donovan, K.A., Dobson, R.C., Wilson, D.J.: Comparing the Conformational Stability of Pyruvate Kinase in the Gas Phase and in Solution. *Journal of the American Society for Mass Spectrometry* **31**, 685-692 (2020)
40. Donor, M.T., Shepherd, S.O., Prell, J.S.: Rapid Determination of Activation Energies for Gas-Phase Protein Unfolding and Dissociation in a Q-IM-ToF Mass Spectrometer. *J. Am. Soc. Mass Spectrom.* **31**, 602-610 (2020)
41. Tesic, M., Wicki, J., Poon, D., K. Y., Withers, S.G., Douglas, D.J.: Gas Phase Noncovalent Protein Complexes that Retain Solution Binding Properties: Binding of Xylobiose Inhibitors to the β -1, 4 Exoglucanase from *Cellulomonas fimi*. *J. Am. Soc. Mass Spectrom.* **18**, 64-73 (2007)
42. Hopper, J.T.S., Oldham, N.J.: Collision Induced Unfolding of Protein Ions in the Gas Phase Studied by Ion Mobility-Mass Spectrometry: The Effect of Ligand Binding on Conformational Stability. *J. Am. Soc. Mass Spectrom.* **20**, 1851-1858 (2009)
43. Liu, L., Michelsen, K., Kitova, E.N., Schnier, P.D., Klassen, J.S.: Energetics of Lipid Binding in a Hydrophobic Protein Cavity. *J. Am. Chem. Soc.* **134**, 3054-3060 (2012)
44. Wolynes, P.G.: Biomolecular folding in vacuo!!!(?). *Proc. Natl. Acad. Sci. U.S.A.* **92**, 2426-2427 (1995)
45. Peschke, M., Verkerk, U.H., Kebarle, P.: Features of the ESI Mechanism that Affect the Observation of Multiply Charged Noncovalent Protein Complexes and the Determination of the Association Constant by the Titration Method. *J. Am. Soc. Mass Spectrom.* **15**, 1424-1434 (2004)
46. Yin, S., Xie, Y., Loo, J.A.: Mass Spectrometry of Protein-Ligand Complexes: Enhanced Gas-Phase Stability of Ribonuclease-Nucleotide Complexes. *J. Am. Soc. Mass Spectrom.* **19**, 1199-1208 (2008)
47. Chen, Y.-R., Deterding, L.J., Sturgeon, B.E., Tomer, K.B., Mason, R.P.: Protein Oxidation of Cytochrome c by Reactive Halogen Species Enhances Its Peroxidase Activity. *J. Biol. Chem.* **277**, 29781-29791 (2002)
48. Lushington, G.H., Cowley, A.B., Silchenko, S., Lukat-Rodgers, G.S., Rodgers, K.R., Benson, D.R.: Comparison of Thioethers and Sulfoxides as Axial Ligands for N-Acetylmicroperoxidase-8: Implications for Oxidation of Methionine-80 in Cytochrome c. *Inorg. Chem.* **42**, 7550-7559 (2003)
49. Wang, Z., Ando, Y., Nugraheni, A.D., Ren, C., Nagao, S., Hirota, S.: Self-oxidation of cytochrome c at methionine80 with molecular oxygen induced by cleavage of the Met-heme iron bond. *Mol. BioSyst.* **10**, 3130-3137 (2014)

50. Birk, A.V., Chao, W.M., Liu, S.Y., Soong, Y., Szeto, H.H.: Disruption of cytochrome c heme coordination is responsible for mitochondrial injury during ischemia. *Biochim. Biophys. Acta* **1847**, 1075-1084 (2015)
51. Capdevila, D.A., Marmisolle, W.A., Tomasina, F., Demicheli, V., Portela, M., Radi, R., Murgida, D.H.: Specific methionine oxidation of cytochrome c in complexes with zwitterionic lipids by hydrogen peroxide: potential implications for apoptosis. *Chem. Sci.* **6**, 705-713 (2015)
52. Nugraheni, A.D., Ren, C.G., Matsumoto, Y., Nagao, S., Yamanaka, M., Hirota, S.: Oxidative modification of methionine80 in cytochrome c by reaction with peroxides. *J. Inorg. Biochem.* **182**, 200-207 (2018)
53. Parakra, R.D., Kleffmann, G.N.L., Jameson, T., Ledgerwood, E.C.: The proportion of Met80-sulfoxide dictates peroxidase activity of human cytochrome c. *Dalton Trans.* **47**, 9128-9135 (2018)
54. Zhong, F., Pletneva, E.V.: Ligation and Reactivity of Methionine-Oxidized Cytochrome c. *Inorg. Chem.* **57**, 5754-5766 (2018)
55. Chea, E.E., Deredge, D.J., Jones, L.M.: Insights on the Conformational Ensemble of Cyt C Reveal a Compact State during Peroxidase Activity. *Biophys. J.* **118**, 128-137 (2020)
56. Barayeu, U., Lange, M., Mendez, L., Arnhold, J., Shadyro, O.I., Fedorova, M., Flemmig, J.: Cytochrome c autocatalyzed carbonylation in the presence of hydrogen peroxide and cardiolipins. *J. Biol. Chem.* **294**, 1816-1830 (2019)
57. Alvarez-Paggi, D., Hannibal, L., Castro, M.A., Oviedo-Rouco, S., Demicheli, V., Tórtora, V., Tomasina, F., Radi, R., Murgida, D.H.: Multifunctional Cytochrome c: Learning New Tricks from an Old Dog. *Chem. Rev.* **117**, 13382-13460 (2017)
58. Veitch, N.C.: Horseradish peroxidase: a modern view of a classic enzyme. *Phytochem.* **65**, 249-259 (2004)
59. McClelland, L.J., Mou, T.-C., Jeakins-Cooley, M.E., Sprang, S.R., Bowler, B.E.: Structure of a mitochondrial cytochrome c conformer competent for peroxidase activity. *Proc. Natl. Acad. Sci. U.S.A.* **111**, 6648-6653 (2014)
60. Kitt, J.P., Bryce, D.A., Minter, S.D., Harris, J.M.: Raman Spectroscopy Reveals Selective Interactions of Cytochrome c with Cardiolipin That Correlate with Membrane Permeability. *J. Am. Chem. Soc.* (2017)
61. Oemer, G., Lackner, K., Muigg, K., Krumschnabel, G., Watschinger, K., Sailer, S., Lindner, H., Gnaiger, E., Wortmann, S.B., Werner, E.R., Zschocke, J., Keller, M.A.: Molecular structural diversity of mitochondrial cardiolipins. *Proc. Natl. Acad. Sci. U.S.A.* **115**, 4158-4163 (2018)

62. Belikova, N.A., Vladimirov, Y.A., Osipov, A.N., Kapralov, A.A., Tyurin, V.A., Potapovich, M.V., Basova, L.V., Peterson, J., Kurnikov, I.V., Kagan, V.E.: Peroxidase Activity and Structural Transitions of Cytochrome c Bound to Cardiolipin-Containing Membranes. *Biochemistry* **45**, 4998-5009 (2006)
63. Yin, V., Mian, S.H., Konermann, L.: Lysine carbonylation is a previously unrecognized contributor to peroxidase activation of cytochrome c by chloramine-T. *Chem. Sci.* **10**, 2349-2359 (2019)
64. Yin, V., Shaw, G.S., Konermann, L.: Cytochrome c as a Peroxidase: Activation of the Pre-Catalytic Native State by H₂O₂-Induced Covalent Modifications. *J. Am. Chem. Soc.* **139**, 15701–15709 (2017)
65. Mushran, S.P., Agrawal, M.C., Prasad, B.: Mechanism of Oxidations by Chloramine-T .1. Oxidation of alpha-hydroxy-acids. *J. Chem. Soc. B* **0**, 1712-1714 (1971)
66. Bachi, A., Dalle-Donne, I., Scaloni, A.: Redox Proteomics: Chemical Principles, Methodological Approaches and Biological/Biomedical Promises. *Chem. Rev.* **113**, 596-698 (2013)
67. Møller, I.M., Rogowska-Wrzesinska, A., Rao, R.S.P.: Protein carbonylation and metal-catalyzed protein oxidation in a cellular perspective. *J. Proteomics* **74**, 2228-2242 (2011)
68. Yang, Y., Stella, C., Wang, W.R., Schoneich, C., Gennaro, L.: Characterization of Oxidative Carbonylation on Recombinant Monoclonal Antibodies. *Anal. Chem.* **86**, 4799-4806 (2014)
69. Konermann, L. Protein Unfolding and Denaturants. In *Encyclopedia of Life Sciences (eLS)*; John Wiley & Sons, Ltd: Chichester, 2012.
70. Haynes, S.E., Polasky, D.A., Dixit, S.M., Majmudar, J.D., Neeson, K., Ruotolo, B.T., Martin, B.R.: Variable-Velocity Traveling-Wave Ion Mobility Separation Enhancing Peak Capacity for Data-Independent Acquisition Proteomics. *Anal. Chem.* **89**, 5669-5672 (2017)
71. Sun, Y., Vahidi, S., Sowole, M.A., Konermann, L.: Protein Structural Studies by Traveling Wave Ion Mobility Spectrometry: A Critical Look at Electrospray Sources and Calibration Issues. *J. Am. Soc. Mass Spectrom.* **27**, 31-40 (2016)
72. Bagel'ova, J., Antalík, M., Tomori, Z.: Effect of polyglutamate on the thermal stability of ferricytochrome c. *Biochem. Mol. Biol. Int.* **43**, 891-900 (1997)
73. Kuroda, Y., Kidokoro, S., Wada, A.: Thermodynamic Characterization of Cytochrome c at Low pH: Observation of the Molten Globule State and of the Cold Denaturation Process. *J. Mol. Biol.* **223**, 1139-1153 (1992)
74. Bushnell, G.W., Louie, G.V., Brayer, G.D.: High-resolution Three-dimensional Structure of Horse Heart Cytochrome c. *J. Mol. Biol.* **214**, 585-595 (1990)

75. de la Mora, F.J.: Electrospray Ionization of large multiply charged species proceeds via Dole's charged residue mechanism. *Anal. Chim. Acta* **406**, 93-104 (2000)
76. Kebarle, P., Verkerk, U.H.: Electrospray: From Ions in Solutions to Ions in the Gas Phase, What We Know Now. *Mass Spectrom. Rev.* **28**, 898-917 (2009)
77. Konermann, L., Metwally, H., Duez, Q., Peters, I.: Charging and Supercharging of Proteins for Mass Spectrometry: Recent Insights into the Mechanisms of Electrospray Ionization. *Analyst* **144**, 6157-6171 (2019)
78. Kaltashov, I.A., Mohimen, A.: Estimates of Protein Surface Area in Solution by Electrospray Ionization Mass Spectrometry. *Anal. Chem.* **77**, 5370-5379 (2005)
79. Mao, Y., Woenckhaus, J., Kolafa, J., Ratner, M.A., Jarrold, M.F.: Thermal unfolding of unsolvated cytochrome c: Experiment and molecular dynamics simulations. *J. Am. Chem. Soc.* **121**, 2712-2721 (1999)
80. Allen, S.J., Schwartz, A.M., Bush, M.F.: Effects of Polarity on the Structures and Charge States of Native-Like Proteins and Protein Complexes in the Gas Phase. *Anal. Chem.* **85**, 12055-12061 (2013)
81. Theisen, A., Black, R., Corinti, D., Brown, J.M., Bellina, B., Barran, P.E.: Initial Protein Unfolding Events in Ubiquitin, Cytochrome c and Myoglobin Are Revealed with the Use of 213 nm UVPD Coupled to IM-MS. *J. Am. Soc. Mass Spectrom.* **30**, 24-33 (2019)
82. Zhao, Q., Schieffer, G.M., Soyk, M.W., Anderson, T.J., Houk, R.S., Badman, E.R.: Effects of Ion/Ion Proton Transfer Reactions on Conformation of Gas-Phase Cytochrome c Ions. *J. Am. Soc. Mass Spectrom.* **21**, 1208-1217 (2010)
83. Lewis, A.K., Dunleavy, K.M., Senkow, T.L., Her, C., Horn, B.T., Jersett, M.A., Mahling, R., McCarthy, M.R., Perell, G.T., Valley, C.r.C., Karim, C.B., Gao, J., Pomerantz, W.C.K., Thomas, D.D., Cembran, A., Hinderliter, A., Sachs, J.N.: Oxidation increases the strength of the methionine-aromatic interaction. *Nat. Chem. Biol.* **12**, 860-866 (2016)
84. Orabi, E.A., English, A.M.: Predicting structural and energetic changes in Met-aromatic motifs on methionine oxidation to the sulfoxide and sulfone. *Phys. Chem. Chem. Phys.* **20**, 23132-23141 (2018)

Table 1. Thermodynamic parameters derived from the thermal unfolding experiments of Figure 3.

	T_M (°C)	ΔH (kJ mol ⁻¹)
Unmodified Control	86.8 ± 0.2	493 ± 20
Fraction I	81.6 ± 0.1	238 ± 4
Fraction II	82.7 ± 0.1	276 ± 6
Fraction III	82.5 ± 0.2	269 ± 8

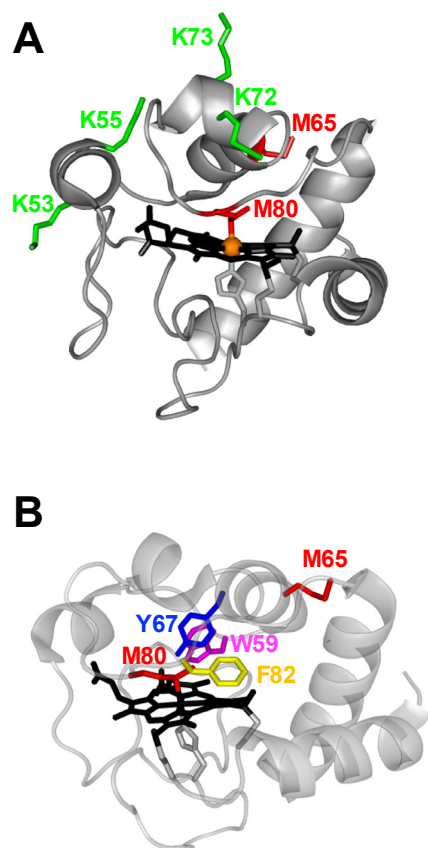


FIGURE 1. Crystal structure of horse cyt *c* (pdb 1hrc). (A) Front view with highlighted side chains that are oxidized after CT exposure: Met (red), and Lys (green). The heme iron is shown in orange. (B) Side view with highlighted Met residues and selected aromatic side chains.

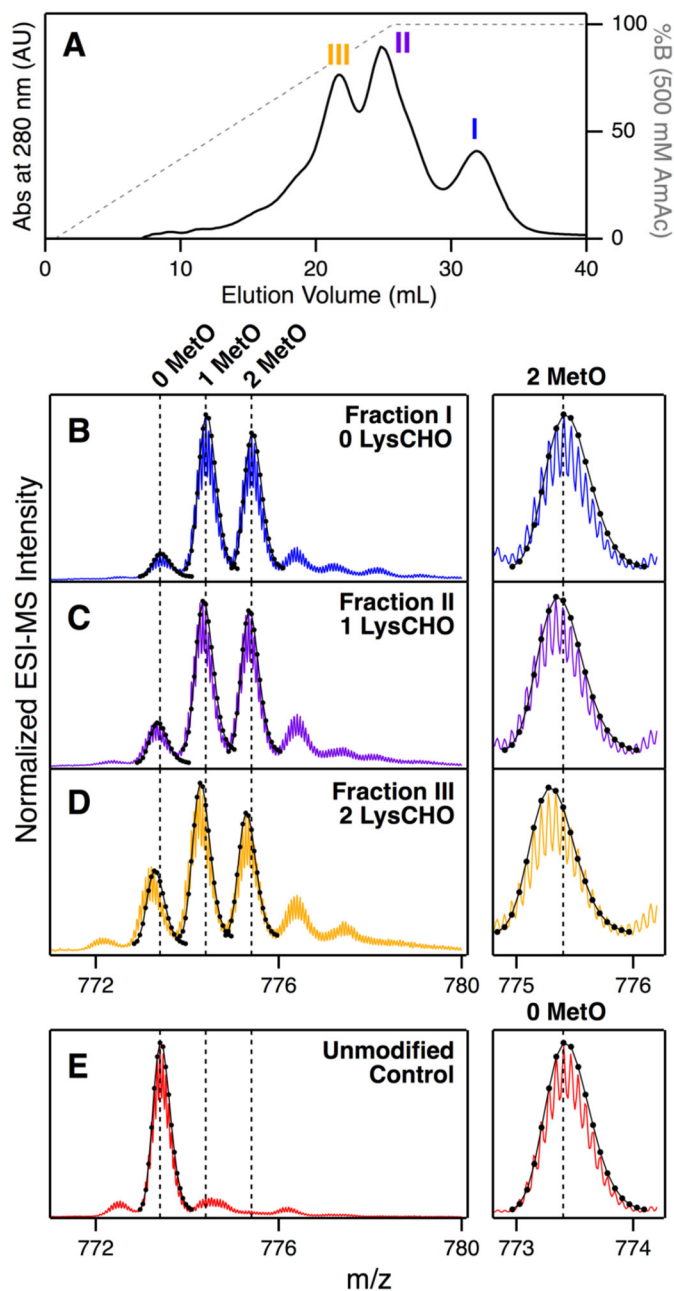


FIGURE 2. SCX fractionation of CT-cyt *c*. (A) Chromatogram after CT exposure; three major fractions I, II, and III are highlighted. (B-D) Mass spectra of the 16+ charge state for each fraction (colored lines), overlaid with isotopic models (black solid lines and dots). (E) Unmodified cyt *c*. The number of MetO and LysCHO modifications for each peak is indicated. Vertical dashed lines were included as a visual aid.

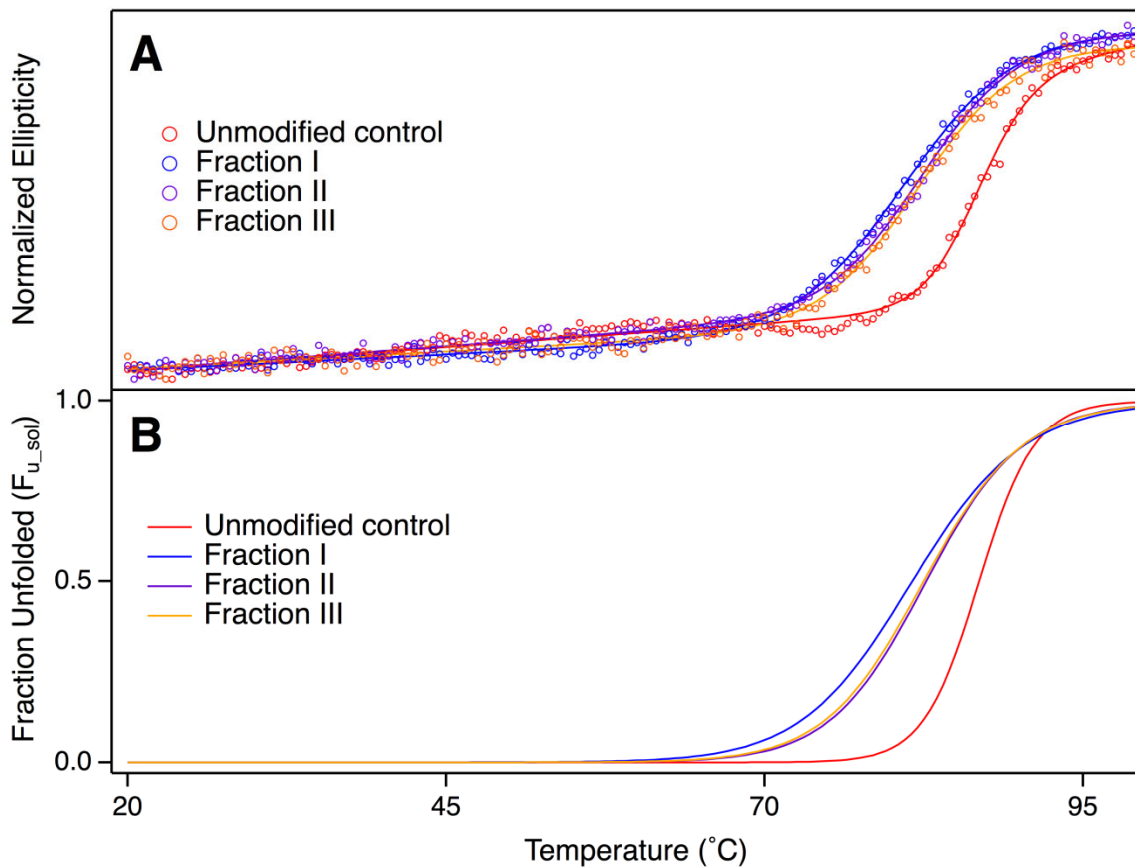


FIGURE 3. Solution phase thermal unfolding of *cyt c* monitored by CD spectroscopy at 222 nm. Data are shown for unmodified control protein, and for fractions I, II, III of CT-*cyt c*. (A) Experimental data points (circles) are overlaid with fits (solid lines) according to Equation 1. T_M and ΔH values derived from these fits are compiled in Table 1. (B) Fraction of unfolded protein in solution (F_{u_sol}) calculated according to Equation 2.

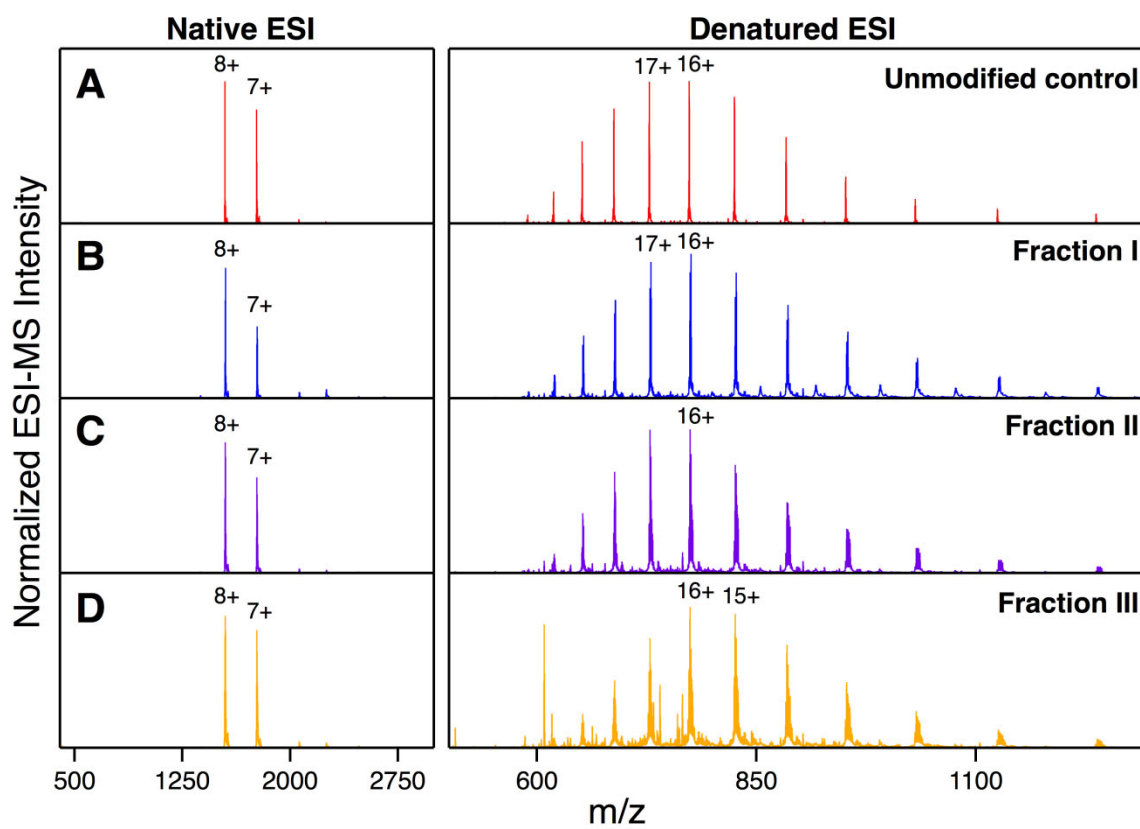


FIGURE 4. Mass spectra of unmodified cyt *c* and the three CT-cyt *c* fractions. Data were acquired under native ESI conditions (left) and under denaturing conditions (right).

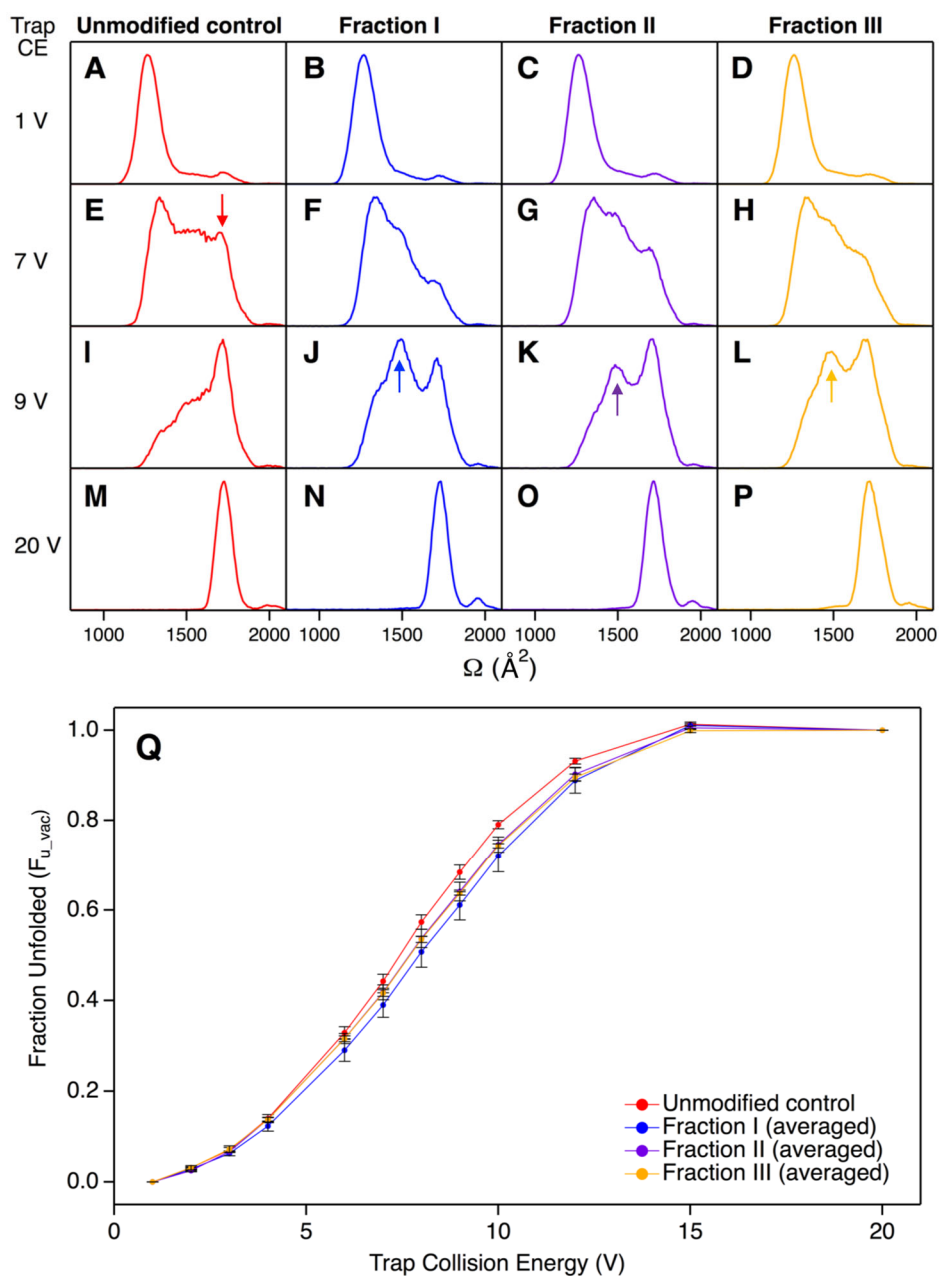


FIGURE 5. CIU of unmodified *cyt c* and CT-*cyt c* fractions I-III for 8+ ions generated by native ESI. The data shown here represent an average of all the MetO isoforms in each fraction. (A-P) IMS profiles acquired at different trap collision energy (Trap CE) values, as indicated along the left hand side. Arrows indicate notable features that are discussed in the text. (Q) CIU unfolding profiles for each type of sample, expressed as F_{u_vac} .

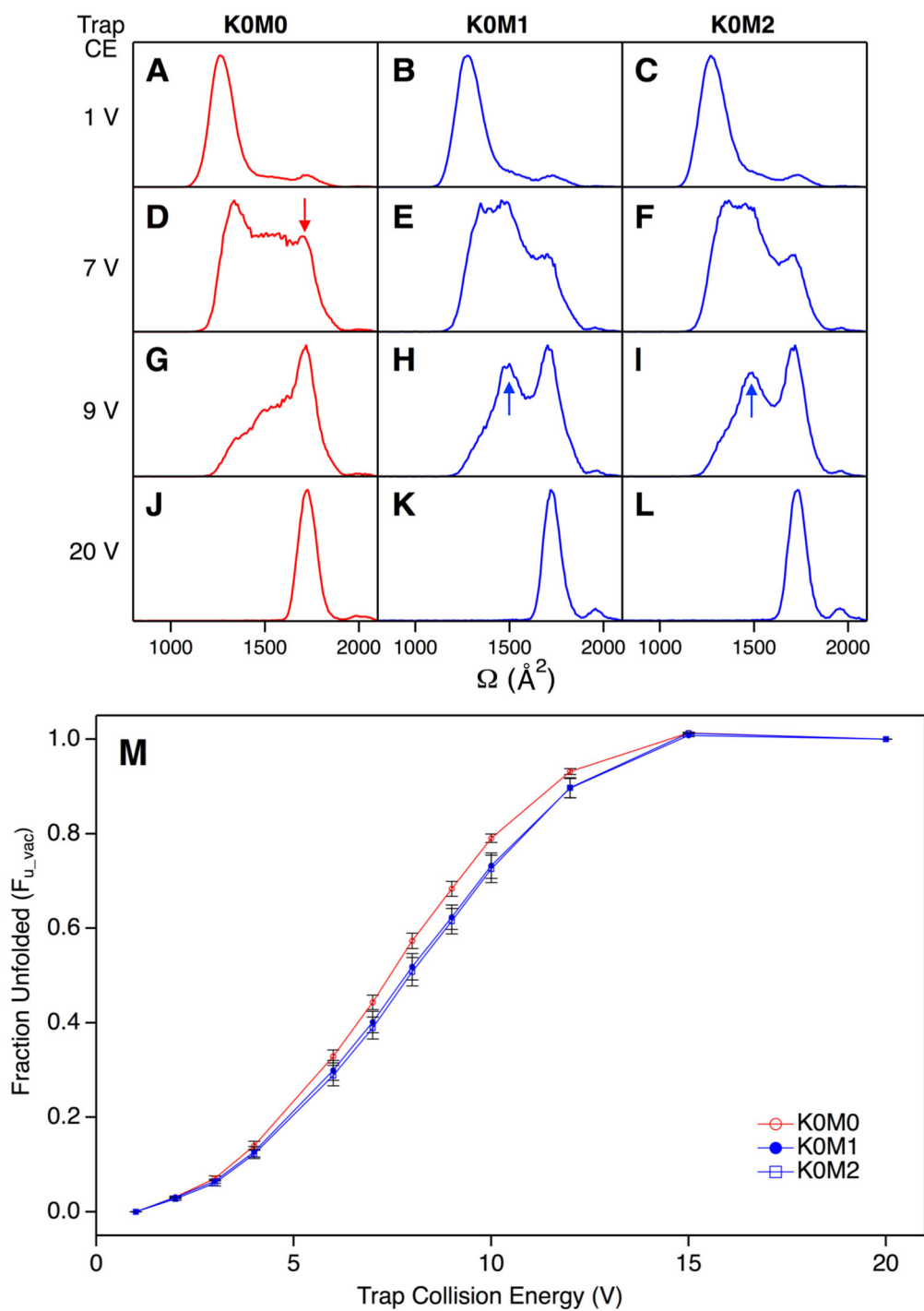


FIGURE 6. CIU of K0Mn proteoforms (zero LysCHO; $n = 0, 1, 2$ MetO) for 8+ ions generated by native ESI. (A-L) IMS profiles for each sample at different trap collision energies. (M) CIU unfolding profiles.

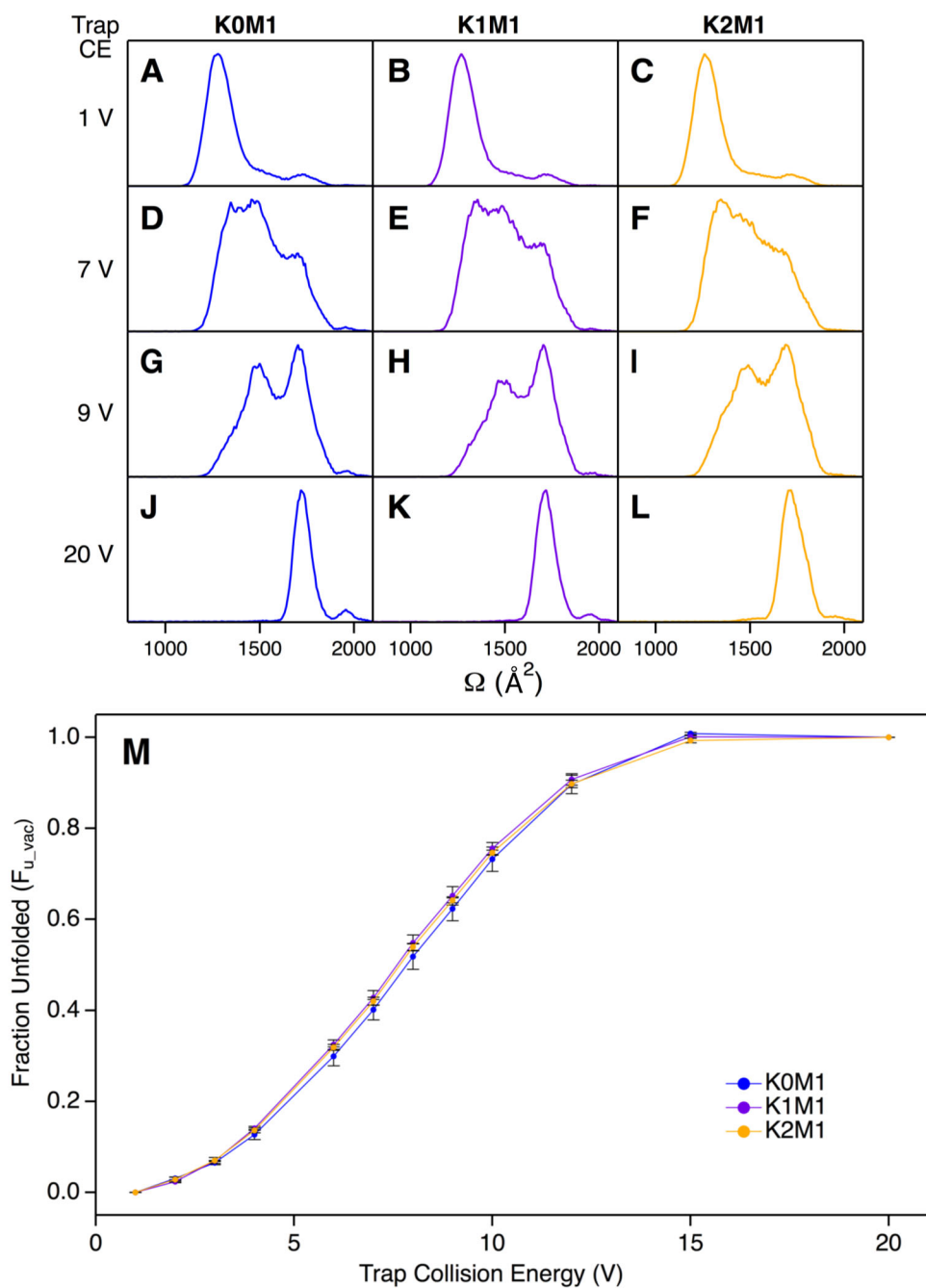
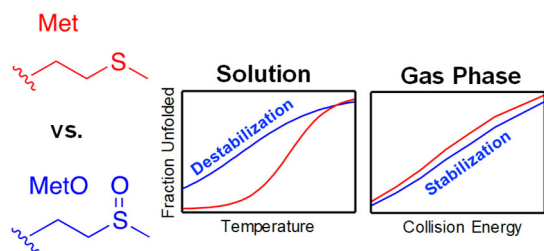


FIGURE 7. CIU of K_mM_1 proteoforms ($m = 0, 1, 2$ LysCHO; 1 MetO) for 8+ ions generated by native ESI. (A-L) IMS profiles for each sample at different trap collision energies. (M) CIU unfolding profiles.

For Table of Contents Only



Probing the Effects of Heterogeneous Oxidative Modifications on the Stability of Cytochrome *c* in Solution and in the Gas Phase

Victor Yin and Lars Konermann

Synopsis: Side chain oxidation reduces protein stability in solution, while slightly enhancing structural resilience in the gas phase.